

A table of numerical values of $Z(p, q)$ is given by Rhodes and Rowlands in the range $0 \leq p \leq 1.1$, $0 \leq q \leq 1.6$.

APPENDIX B

Consider an arbitrarily shaped body uniformly magnetized in the x direction. Let dS_1 , dS_2 be two elements of area about points P_1 , P_2 on its surface, and $d\mathbf{S}_1$, $d\mathbf{S}_2$ the corresponding vector areas. The elementary "magnetic charges" about P_1 , P_2 are $\mathbf{I} \cdot d\mathbf{S}_1 = IdS_{1x}$, $\mathbf{I} \cdot d\mathbf{S}_2 = IdS_{2x}$, respectively. Denoting the distance $|P_1P_2|$ by $r_{12} = r_{21}$, we may express the total magnetostatic energy as

$$W_x = \frac{1}{2} I^2 \oint \frac{dS_{1x} dS_{2x}}{r_{12}}, \quad \text{i.e.,} \quad N_x = \frac{1}{v} \oint \frac{dS_{1x} dS_{2x}}{r_{12}}.$$

If x , y , z are three mutually perpendicular axes, we have

$$N_x + N_y + N_z = \frac{1}{v} \oint \frac{d\mathbf{S}_1 \cdot d\mathbf{S}_2}{r_{12}}. \quad (\text{B1})$$

We shall now use the vector identity⁸

$$\int d\mathbf{S} \star \Phi = \frac{1}{v} \int d\tau \nabla \star \Phi,$$

where Φ may be a scalar, a vector, or a tensor (dyadic) and where the star stands for a dot product, a cross product, or an ordinary multiplication. Taking the origin at P_1 and allowing P_2 to be any point of the body, we have

$$\int \frac{d\mathbf{S}_2}{r_{12}} = \int d\tau_2 \nabla_2 \left(\frac{1}{r_{12}} \right) = - \int d\tau_2 \frac{\mathbf{r}_{12}}{r_{12}^3} = \int d\tau_2 \frac{\mathbf{r}_{21}}{r_{12}^3}.$$

The integral in (B1) may thus be rewritten as

$$\int \frac{d\mathbf{S}_1 \cdot d\mathbf{S}_2}{r_{12}} = \int d\tau_2 \int \frac{d\mathbf{S}_1 \cdot \mathbf{r}_{21}}{r_{21}^3} = \int d\tau_2 (4\pi) = 4\pi v,$$

and (B1) leads to Eq. (2) of the text, namely, $N_x + N_y + N_z = 4\pi$.

⁸ H. B. Phillips, *Vector Analysis* (John Wiley and Sons, Inc., New York, 1933), p. 72, Eq. (127).

Large-Signal Surface Photovoltage Studies with Germanium

E. O. JOHNSON

RCA Laboratories, Princeton, New Jersey

(Received July 2, 1957)

Studies of the surface photovoltage of germanium were carried out over a considerably wider range of excess carrier densities than previously reported. Ambient induced inversion and accumulation layer surfaces were studied on p - and n -type Ge with resistivities ranging from 1 to 15 ohm-cm. The photovoltage was measured with ac methods and the excess carrier density was monitored by changes in the specimen conductance. The observed dependence of the photovoltage on the excess carrier density agreed quite well with theory that considers the surface space charge, but neglects charge changes in fast surface states. Comparison of the observed and theoretical curves is believed to give the surface potential to within about one kT/e unit for potentials

less than about $8kT/e$ units, even if the effect of previously reported fast states is neglected. Excursions of the surface potential over the ambient cycle were found to be about the same as those reported for other types of surface measurements.

The large signal photovoltage, in the range of surface potentials covered in the present work, is insensitive to fast states having the range of parameters extant in the literature: sensitivity is largely restricted to unreported parameter values. Since no evidence for fast states was observed in the present experiments, it is concluded that the present results are at least consistent with previously reported fast-state parameter values.

I. INTRODUCTION

THE model shown in Fig. 1 is the presently accepted one for semiconductor surfaces.¹ Electric charge represented by Σ_{ss} and Σ_{fs} is immobilized at the surface in two different types of surface states. The first type of state, called "slow," is located on or within the surface oxide layer. These states are affected by the ambient atmosphere and usually contain a relatively large amount of charge. Charge exchange with the bulk occurs slowly, with time constants of the order of

seconds. The model in the figure applies for n -type material where the slow-state charge Σ_{ss} is negative and the whole system is in thermal equilibrium with no injected carriers present. The second type of trap state is considered as existing at the interface between the oxide and the bulk material. These states, with a charge Σ_{fs} , are called "fast" because the charge transfer between them and the bulk is measured in times of the order of microseconds, or less. These states are thought to be relatively independent of ambient changes and also to be associated with the surface recombination of holes and electrons.

¹ R. H. Kingston, *J. Appl. Phys.* **27**, 101 (1956).

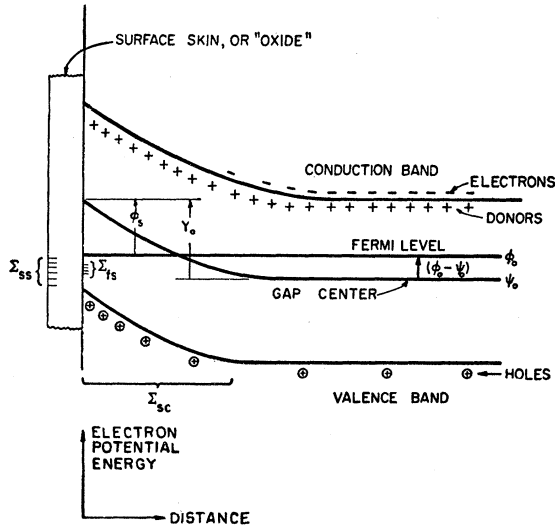


FIG. 1. Diagram of semiconductor surface.

The algebraic sum of charge in these two types of states is balanced by a charge of donors, acceptors, free holes, and free electrons existing in a layer extending into the bulk material for a distance of 10^{-6} to 10^{-4} cm. This aggregate charge, denoted by Σ_{sc} in the figure, is known as the surface space charge. The equilibrium electrostatic potential across the space-charge layer, denoted by Y_0 , is known as the surface potential. In many cases it is convenient to relate Y_0 to the bulk Fermi level and the midgap potential by the quantity ϕ_s which is shown in the figure and defined in Table I. The other symbols in the figure are also defined in Table I along with various other symbols to be used in the analysis.

Studies of the electrical properties of semiconductor surfaces have been concerned with determinations of the surface potential and the energy levels and densities of both types of surface states. In such studies the surface is often "biased" by an ambient cycle that changes the charge in the slow states between positive and negative extremes. The desired surface parameters can be deduced from different experimental techniques which include field effect,¹⁻³ channel,^{4,5} back-surface diode,⁶ and photovoltage measurements.⁷⁻⁹ The first two yield information through changes in the conductivity of the bulk material in the layers adjacent to the

surface. There is some uncertainty in this information because the carrier mobilities in these surface layers have never been directly determined. Virtually all of the data on the fast surface states have been determined by these methods. The third method is independent of mobility considerations and is presently being studied in these laboratories.

The fourth and last technique, the subject of this paper, also has the advantage that it is independent of surface mobility considerations. To implement this technique the surface is illuminated with light chopped at a rate (~ 60 cps) so rapid that the charge Σ_{ss} does not have time to change. Assume for the moment that charge changes in the fast states can be neglected. Then, since over-all electrical neutrality must be preserved, the introduction of the light-injected carriers cannot produce a net charge change in the space charge but, instead, will cause a charge redistribution. Associated with this is a change in the surface potential. This change in potential, defined as ΔY in Table I and called the surface photovoltage, is picked up by an electrode located close to the surface. From a knowledge

TABLE I. Symbols.

Σ_{ss}	= number of electron charge units per cm^2 of surface in slow states.
Σ_{fs}	= number of electron charge units per cm^2 of surface in fast states.
Σ_{sc}	= number of electron charge units per cm^2 of surface in the space charge.
ψ	= electrostatic potential.
Y	= electrostatic potential, in kT/e units, across the surface space-charge region. This has a negative value if the energy bands bend upwards in the conventional band picture, and a positive value if the bend is downwards. Y_0 refers to the equilibrium value of Y .
$\Phi_s = Y - \ln \Lambda$. This potential is frequently referred to as the surface potential.
$\Delta Y = Y - Y_0$, the surface photovoltage.
$\Lambda = (p_0/n_0)^{1/2} = p_0/n_i = n_i/n_0 = e^{B(\Phi_s - \psi_0)}$.
Φ_n	= the quasi-Fermi level for electrons, assumed to be constant across the space-charge region.
Φ_p	= the quasi-Fermi level for holes, assumed to be constant across the space-charge region.
Φ_0	= the Fermi level deep in the bulk where equilibrium conditions exist.
ϵ	= the dielectric constant.
$P = B(\Phi_p - \Phi_0)$.
$N = B(\Phi_n - \Phi_0)$.
$B = e/kT$, where e is the absolute value of the electron charge and k and T have their usual meanings.
$L = [\epsilon/2\pi em_i B]^2$, a characteristic length differing only slightly from the Debye length. At room temperature $L = 1.4 \times 10^{-4}$ for Ge, and 5.8×10^{-3} for Si.
n_0	= free electron density deep in the bulk.
p_0	= free hole density deep in the bulk.
n_i	= intrinsic carrier density. At room temperature $n_i = 2.5 \times 10^{13}$ for Ge, and 6.8×10^{10} for Si.
n_s, p_s	= surface densities of free electrons and holes.
n_1, p_1	= equilibrium electron and hole surface densities for the case where the Fermi level passes through the trap energy level.
$\Delta n, \Delta n_1, \Delta p, \Delta p_1$	= fractional increase in the minority, electron, and hole carrier densities due to injection.
$C_n = N_i v_n \sigma_n$; $C_p = N_i v_p \sigma_p$, where N_i is the fast-state density per cm^2 of surface, v_n and v_p are the thermal speeds for electrons and holes, and σ_n and σ_p are the fast trap capture cross sections for electrons and holes, respectively.

² H. C. Montgomery and W. L. Brown, Phys. Rev. **103**, 865 (1956).

³ S. Wang and G. Wallis, Phys. Rev. **105**, 1459 (1957).

⁴ Statz, deMars, Davis, and Adams, Phys. Rev. **101**, 1272 (1956).

⁵ Statz, deMars, Davis, and Adams, Phys. Rev. **106**, 455 (1957).

⁶ J. E. Thomas, Jr., and R. H. Rediker, Phys. Rev. **101**, 984 (1956).

⁷ W. H. Brattain and J. Bardeen, Bell System Tech. J. **32**, 1 (1953).

⁸ C. G. B. Garrett and W. H. Brattain, Phys. Rev. **99**, 376 (1955).

⁹ W. H. Brattain and G. C. B. Garrett, Bell System Tech. J. **35**, 1019 (1956).

of the photovoltage and the fractional increase Δ_m in the minority carrier density, due to the light, it is possible to deduce the value of Y_0 . Previous determinations of Y_0 by this method were made at low light levels where the concern was with differential variations of Y .⁷⁻⁹ These give a limited amount of information about the surface unless they are combined with other types of measurements.⁹ It seemed expedient, therefore, to obtain more information by undertaking a study of the variation of the surface photovoltage over a wide range of the minority carrier injection factor Δ_m .¹⁰ This should show, first of all, how well the observed photovoltages agree with theoretical prediction. Secondly, it should show the role played by the fast surface states and possibly give information about the density and energy levels of these states.

In this paper the large signal photovoltage as a function of the minority carrier injection factor is first derived with neglect of charge changes in the fast surface states. The effect of charge change in the fast states is then introduced by means of a graphical treatment. The experimental techniques are described in the following sections and the results compared with theory. The results and conclusions from the present work are then discussed and compared with those obtained from the other types of surface measurements.

II. THEORY

The symbols to be used in the treatment of the space charge region are those of Brattain and Garrett.⁸ These are listed in Table I and some are illustrated, along with other symbols to be used, in Fig. 1. For convenience, the relation between Λ and resistivity for germanium at room temperature is plotted in Fig. 2.

Solution of Poisson's equation, using the usual Boltzmann relations for free electron and hole densities, gives the electric field at the surface edge of the space region as⁸

$$\frac{d\psi}{dx} = \left[\frac{2}{BL} \right] F = 370F \text{ for Ge} \quad (1)$$

$$= 8.93F \text{ for Si,}$$

where F , the space-charge factor, is a dimensionless quantity given by

$$F = \mp [\Lambda e^P (e^{-Y} - 1) + \Lambda^{-1} e^{-N} (e^Y - 1) + (\Lambda - \Lambda^{-1}) Y]^{\frac{1}{2}}. \quad (2)$$

The sign convention is such that the negative sign is used when $Y < 0$, and the positive sign when $Y > 0$. The first term on the right accounts for the hole charge, the second for the electron charge, and the third accounts for the charge due to donors and acceptors. It has been assumed that all donors and acceptors are ionized and that the carrier diffusion length considerably exceeds the width of the space-charge region ($\sim 10^{-4}$ cm).

The surface field can be converted to the surface

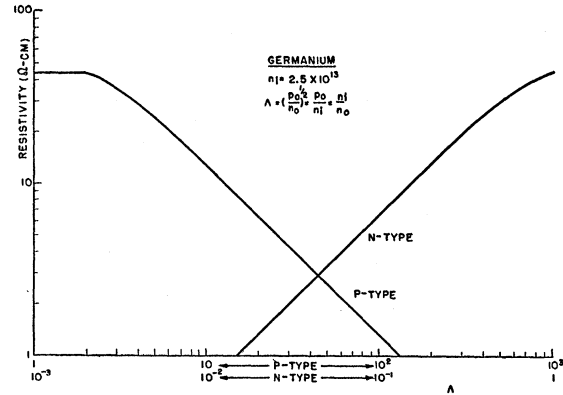


FIG. 2. Relation between Λ and resistivity for Ge.

space charge Σ_{sc} per square cm of surface area by Gauss' theorem which gives

$$\Sigma_{sc} = [n_i L] F = 3.5 \times 10^9 F \text{ for Ge} \quad (3)$$

$$= 3.94 \times 10^7 F \text{ for Si.}$$

It is a straightforward matter to show that

$$e^P = 1 + \Delta_p, \quad e^{-N} = 1 + \Delta_n, \quad \Lambda^2 \Delta_p = \Delta_n, \quad (4)$$

where Δ_p and Δ_n are the fractional changes in hole and electron densities caused by light injected carriers. In the last expression it has been assumed that the change in electron and hole density caused by injection is equal. These relations are valid for any value of Δ_p or Δ_n . Using the above relations the space-charge factor is converted to

$$F = \mp [\Lambda (e^{-Y} - 1) + \Lambda^{-1} (e^Y - 1) + (\Lambda - \Lambda^{-1}) Y + \Lambda (e^Y + e^{-Y} - 2) \Delta_p]^{\frac{1}{2}}. \quad (5)$$

If there are no light-injected carriers, the last group of terms disappears. The resulting value of F , the non-injection value, will be designated as F_0 . This is plotted in Fig. 3 as a function of Y_0 for depletion and inversion layers and in Fig. 4 for accumulation layers.¹¹ The symmetry of the function F_0 with respect to Λ and Y_0 makes it possible to handle both n - and p -type material with only two sets of curves. To use the curves with p -type material use the values and Y_0 polarities as shown. With n material the reciprocal of Λ is taken along with a reversal in the polarity of Y_0 .

The shape of the space-charge curves is easily understood. For intrinsic material the space charge arises essentially from one sign of carrier and increases exponentially with surface potential. It thus appears as a straight line on the semilogarithmic plot, except for the region close to $Y_0 = 0$. The gently sloping plateau on the curves in Fig. 3 arises from fixed donor or acceptor charge and corresponds to the region where the Schottky depletion-layer treatment is valid. The

¹⁰ E. O. Johnson, Bull. Am. Phys. Soc. Ser. II, 2, 66 (1957).

¹¹ R. H. Kingston and S. F. Neustadter, J. Appl. Phys. 26, 718 (1955).

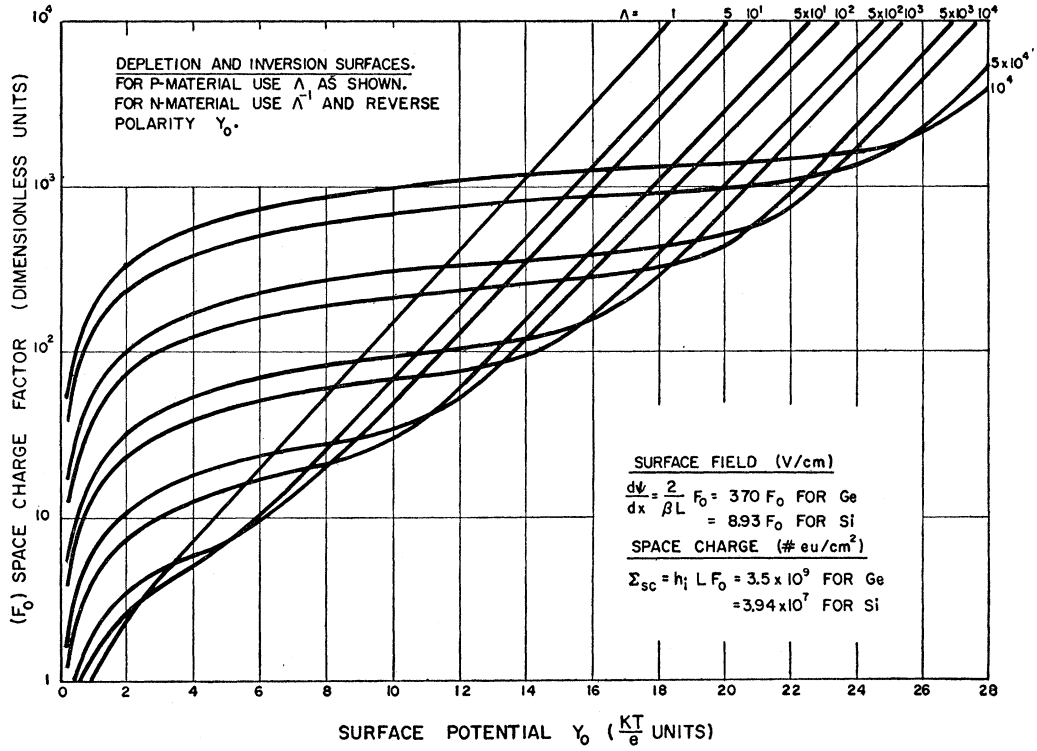


FIG. 3. Space-charge factor F_0 as a function of surface potential for inversion layers.

knee on this plateau occurs at roughly one kT/e unit of surface potential. This potential is sufficient to reduce the majority carrier charge, opposite in sign to

the fixed charge, to a significantly smaller value. The plateau disappears at high surface potentials due to the minority carrier charge which increases exponentially. This charge becomes dominant at higher surface potentials in heavily doped material because of lower bulk minority carrier density. This causes the curves to cross. The curves do not cross, however, if ϕ_s is used on the abscissa instead of Y_0 .¹¹ The accumulation-layer curves show more charge than the inversion-layer ones because the majority carrier charge is involved. The knee in these curves also occurs close to one kT/e unit of surface potential because this potential is sufficient to make the majority carrier charge increase significantly above the fixed donor or acceptor charge.

Charge neutrality requires that

$$\Sigma_{ss} + \Sigma_{fs} + \Sigma_{sc} = 0. \tag{6}$$

If Σ_{fs} is neglected and the carriers are injected at the surface at a rate fast compared to the time constant for Σ_{ss} , then Σ_{ss} , and hence Σ_{sc} , will remain constant during an injection pulse. Consequently, relation (5) and the definition

$$F_Y^2 = \Lambda(e^{-Y} - 1) + \Lambda^{-1}(e^Y - 1) + (\Lambda - \Lambda^{-1})Y, \tag{7}$$

give

$$\Delta_p = \frac{F_0^2 - F_Y^2}{\Lambda(e^Y + e^{-Y} - 2)}. \tag{8}$$

It is more convenient to plot this expression directly,

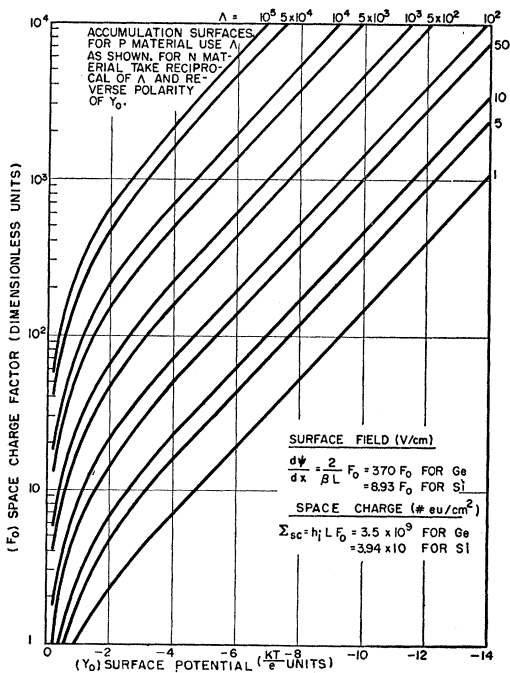


FIG. 4. Space-charge factor F_0 as a function of surface potential for accumulation layers.

rather than to try to get an implicit expression for Y and hence $Y - Y_0 = \Delta Y$, the surface photovoltage. Both Eqs. (5) and (8) can be expressed in terms of Δ_n by use of the last relation in (4).

If the exponential terms dominate in F_0 and F_Y in Eq. (8), and the surface potential has an intermediate value between zero and Y_0 , the photovoltage is a logarithmic function of the injection factor. The relationship between the photovoltage and the injection factor is a linear one if the photovoltage is less than about $0.05kT/e$ unit.¹² The symmetry between surface potential and Λ facilitates plotting the surface photovoltage ΔY as a function of the injection parameter. The curves for intrinsic material, where $\Lambda = 1$, are shown in Fig. 5. These curves also apply to accumulation layers if the majority-carrier injection factor is used on the horizontal axis. If the minority-carrier injection factor is used, the values along the abscissa must be multiplied by the factor Λ^2 . Characteristics of surfaces tending toward inversion, with $\Lambda = 10^2$ and

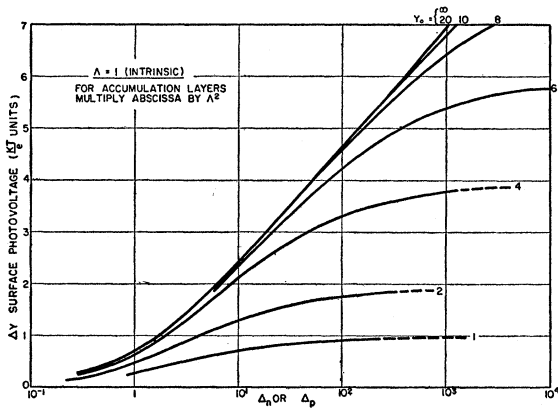


FIG. 5. Surface photovoltage as a function of carrier injection for $\Lambda = 1$.

10^4 , are shown in Figs. 6 and 7. In these figures the abscissa refers to the minority-carrier injection factor. It will be noted that a curve for a particular value of Y_0 asymptotically approaches the same absolute value of ΔY at high injection levels. This is a manifestation of the fact that the surface potential Y approaches zero at high injection levels.

As might be intuitively expected from viewing the surface space region as a "quasi-junction," there is a very close similarity between the surface photovoltage and the photovoltaic effect at a junction.¹³ In fact, the surface and junction photovoltages are identical functions of excess carrier density, the saturation regions excepted.

¹² This offers the possibility of measuring the minority carrier lifetimes with the surface photovoltage. The technique has the outstanding advantage that no physical contact need be made to the specimen; all contacts can be capacitive. See E. O. Johnson, J. Appl. Phys. 28, 1349 (1957).

¹³ I am indebted to J. Loferski and P. Rappaport for bringing this to my attention.

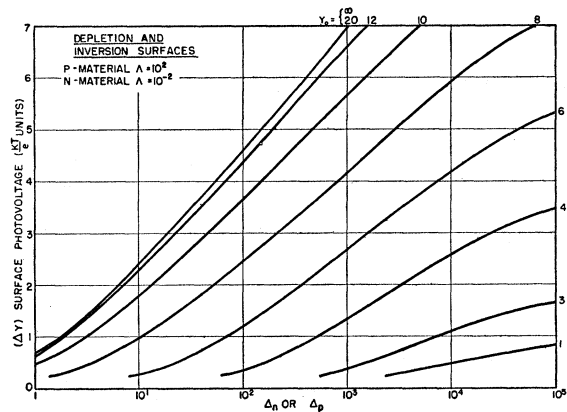


FIG. 6. Surface photovoltage as a function of carrier injection for $\Lambda = 10^2$.

The preceding mathematical treatment, leading to Eq. (8), expresses the physical fact that the surface potential must decrease if the net charge in the surface space-charge region is to remain constant. In the particular case shown in Fig. 1, for example, the net charge in the space-charge region would increase with injection, due to the increase in hole charge, if the surface potential remained constant. The potential ΔY for the case where Σ_{sc} remains constant, arises from the space-charge redistribution that takes place during injection.

The relation between the injection and the surface photovoltage can be derived in a graphical way that more clearly brings out the physical relations, particularly when Σ_{ss} changes or appears to change because of a change of charge in the fast states. Consider Fig. 8 which applies to n -type Ge with $\Lambda = 10^{-1}$. Here the space charge function F , as given by Eq. (5), is plotted as a function of the surface potential Y with the hole injection ratio Δ_p as the variable parameter. The curve with $\Delta_p = 0$ is identical to the $\Lambda = 10$ curve in Fig. 3. The other curves can be understood from the fact that an increase in the hole density with injection causes

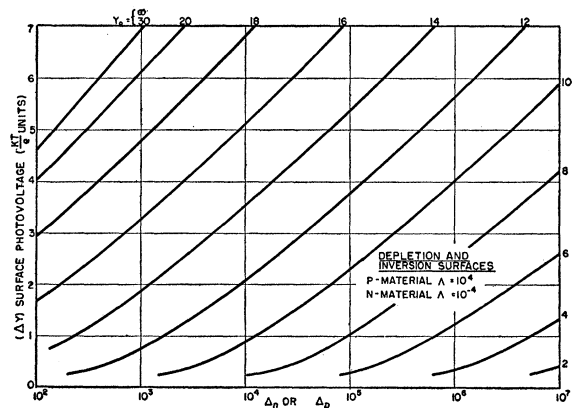


FIG. 7. Surface photovoltage as a function of carrier injection for $\Lambda = 10^4$.

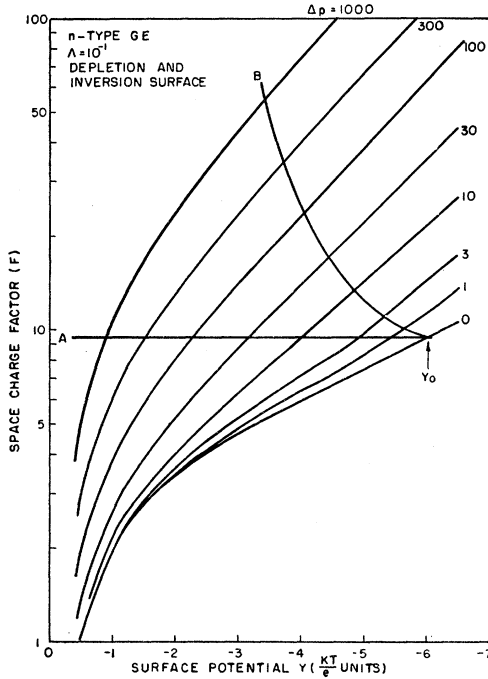


FIG. 8. Space-charge factor F as a function of injection. $\Lambda = 10^{-1}$, n -type Ge.

the hole charge in the space-charge region to predominate at lower surface potentials. For the case where there are no fast states and the slow-state charge Σ_{ss} remains constant with injection, the system must move along a horizontal line. The line A applies to the particular case where $Y_0 = -6$. The values of the surface potential for different values of Δ_p are described by the intersections of line A with the F curves. The quantity $\Delta Y = Y - Y_0$ is the photovoltage. The curves shown in Figs. 5, 6, and 7 could have been constructed in this manner. If either Σ_{ss} or Σ_{fs} changes during the injection cycle, the system will move along some line other than A , the line B , for example. It is easy to see, depending upon the path that the system takes, that the surface potential could change more slowly or more rapidly with injection than for the case of line A . In fact, ΔY could remain constant or even change sign as the injection increases. Most of the various possibilities have been observed. However, as noted later, in all the cases observed so far these peculiarities could be accounted for by charge changes in the slow states.

Restricting our attention to states located at a discrete energy level, the number of electron charges per square centimeter of surface in fast traps is

$$\Sigma_{fs} = N_t f,$$

where N_t is the fast-state density per cm^2 of surface and f is the electron occupancy factor. The occupancy factor f is derived from the Shockley-Read treatment.¹⁴

¹⁴ W. Shockley and W. T. Read, Jr., Phys. Rev. **87**, 835 (1952).

The form appropriate for the surface is

$$f = \frac{C_n n_s + C_p p_l}{C_n (n_s + n_l) + C_p (p_s + p_l)},$$

where the various quantities are defined in Table I. An expression for f in terms of the energies of the fast states, the injection ratios, and the surface potential, can be derived¹⁵ by using the definition $\chi^2 = C_p/C_n$, and the relations

$$n_l = n_i e^{-\nu}, \quad p_l = n_i e^{\nu},$$

where ν is the energy difference, in kT/e units, of the trap level from the middle of the forbidden band. The quantity is positive when the traps are below gap center, and negative when above. The resulting expression is

$$f = \left[1 + (1 + \Delta_p) e^{-(Y - \ln \Lambda + \nu)} - \frac{\Delta_p + \Delta_n + \Delta_p \Delta_n}{(1 + \Delta_n) e^{(Y - \ln \Lambda + \nu)} + \chi^2 e^{2\nu}} \right]^{-1}. \quad (9)$$

The definition

$$T = \frac{\chi^2 e^{2\nu} e^{-(Y - \ln \Lambda + \nu)}}{1 + \Lambda^2 \Delta_p},$$

and Eq. (9) lead to

$$f = \left[1 + e^{-(Y - \ln \Lambda + \nu)} \left(\frac{1 + T(1 + \Lambda^2 \Delta_p)(1 + \Delta_p)}{(1 + T)(1 + \Lambda^2 \Delta_p)} \right) \right]^{-1}. \quad (10)$$

It is immediately seen that f reduces to the familiar Fermi factor if there is no injection. The effect of injection on f depends upon the factor T . If $T \gg 1$, Eq. (10) reduces to

$$f = [1 + (1 + \Delta_p) e^{-(Y - \ln \Lambda + \nu)}]^{-1}, \quad (11)$$

and injection tends to decrease f . If $T \ll 1$, Eq. (10) reduces to

$$f = \left[1 + \left(\frac{1}{1 + \Lambda^2 \Delta_p} \right) e^{-(Y - \ln \Lambda + \nu)} \right]^{-1}, \quad (12)$$

and injection tends to increase f . This behavior is easily understood in terms of the capture cross-section ratio χ^2 . The use of the above limiting forms of Eq. (10) facilitates calculation. On an f vs Y diagram it is found that the occupancy curve retains its general shape with injection, but is translated along the Y axis in a direction that depends upon which extreme value of T is used.

III. EFFECT OF FAST STATES ON THE SURFACE PHOTOVOLTAGE

It is a straightforward, but tedious, process to evaluate the effect of fast states on the surface photo-

¹⁵ C. G. B. Garrett and W. H. Brattain, Bell System Tech. J. **35**, 1041 (1956).

TABLE II. Effect of fast states on surface photovoltage in *n*-type Ge, $\Lambda=10^{-1}$.

Case	ν	T	χ^2	N_t	Y_0	Effect on ΔY vs Δ_p curve (relative to $N=0$ case)
1	6	$\gg 10$	$>10^{-1}$	10^{12}	-6	Small upward displacement, undetectable
2	6	$\gg 10$	$>10^{-1}$	10^{11}	-6	Small upward displacement, undetectable
3	6	$\gg 10$	$>10^{-1}$	10^{11}	-3	Small upward displacement, undetectable
4	5	$\gg 10$	>1	10^{12}	-6	Small upward displacement, undetectable
5	5	$\gg 10$	>1	10^{11}	-6	Small upward displacement, undetectable
6	5	$\gg 10$	>1	10^{12}	-4	Small upward displacement, undetectable
7	5	$\gg 10$	>1	10^{11}	-4	Small upward displacement, undetectable
8	4	$\gg 10$	>3	10^{12}	-6	Small upward displacement, undetectable
9	4	$\gg 10$	>3	10^{11}	-6	Small upward displacement, undetectable
10	2	$\gg 10$	>10	10^{12}	-6	Small upward displacement, undetectable
11	2	$\gg 10$	>10	10^{11}	-6	Small upward displacement, undetectable
12	6	$\ll 1$	$<10^{-7}$	10^{12}	-6	Large downward displacement with steep rise at end, detectable
13	6	$\ll 1$	$<10^{-7}$	10^{11}	-6	Small downward displacement, undetectable
14	2	$\ll 1$	$<10^{-4}$	10^{11}	-6	Large downward displacement with rise at end, detectable
15	-4	$\ll 1$	$<10^{-1}$	10^{12}	-6	Marked droop beyond $\Delta_p=10$, detectable
16	-4	$\ll 1$	$<10^{-1}$	10^{11}	-6	Marked droop beyond $\Delta_p=10^2$, detectable
17	-4	$\gg 10$	$>10^6$	10^{11}	-6	No effect, states remain empty
18	-6	$\ll 1$	<2	10^{12}	-6	Droop beyond $\Delta_p=10^2$, detectable
19	-6	$\ll 1$	<2	10^{11}	-6	Very little effect
20	4	$\gg 10$	$>10^3$	10^{11}	4	No effect, states remain filled
21	4	$\gg 10$	$>10^3$	10^{11}	2	Marked droop at beyond $\Delta_p=10^2$, detectable
22	-4	$\gg 10$	$>10^6$	10^{11}	2	Reversal of polarity, easily detectable
23	-4	$\ll 1$	<1	10^{11}	2	Very little effect

voltage. The possible combinations of the various parameters are legion so that only the representative sampling listed in Tables II and III was made. The computations were carried out as follows:

- (1) The space-charge curves, such as shown in Fig. 8, were constructed for both inversion- and accumulation-layer conditions for the particular specimen to be considered.
- (2) Universal tables of values for f from Eqs. (11) and (12) were constructed.
- (3) A particular set of values of ν , T , N_t , and Y_0 , such as listed in Table II or III, was chosen. These

quantities fix the zero-injection values of F and f , and hence Σ_{sc} and Σ_{fs} . The slow-state charge is then fixed by Eq. (6).

(4) Starting with the zero-injection values of the various quantities noted in (3) one can conveniently proceed with the plotted space-charge curves to get a graphical solution for Y at each value of injection, such that Eq. (6) is always satisfied. The photovoltage, $\Delta Y=Y-Y_0$, is thus determined at each value of injection.

The slow-state charge is assumed to remain constant over an injection cycle. The final results are not affected

TABLE III. Effect of fast states on surface photovoltage in *p*-type Ge, $\Lambda=10$.

Case	ν	T	χ^2	N_t	Y_0	Effect on ΔY vs Δ_n curve (relative to $N=0$ case)
1	>9	$\gg 10$	$>10^{-1}$	10^{12}	1-6	None, states remain filled
2	8	$\gg 10$	>1	10^{12}	6	Small droop at $\Delta_n=10^3$, undetectably small
3	6	$\gg 10$	>1	10^{12}	6	Pronounced droop beyond $\Delta_n=10^2$, detectable
4	6	$\gg 10$	>1	10^{11}	6	Small effect, not detectable
5	5	$\gg 10$	>10	3×10^{11}	6	Small droop near $\Delta_n=10^3$, possibly detectable
6	5	$\gg 10$	>10	10^{11}	6	Very small droop at $\Delta_n=10^3$, not detectable
7	5	$\gg 10$	>10	3×10^{11}	4	Droop near $\Delta_n=10^3$, just detectable
8	5	$\gg 10$	>10	10^{11}	4	Very small droop near $\Delta_n=10^3$, not detectable
9	4	$\gg 10$	>30	10^{12}	6	Pronounced droop beyond $\Delta_n=10^2$, detectable
10	4	$\gg 10$	>30	10^{11}	6	Small droop beyond $\Delta_n=10^2$, possibly detectable
11	2	$\gg 10$	$>10^2$	10^{12}	6	Droop beyond $\Delta_n=10^2$, detectable
12	2	$\gg 10$	$>10^2$	10^{11}	6	Droop beyond $\Delta_n=10^2$, detectable
13	4	$\gg 10$	>30	10^{12}	-3	Very slight effect
14	4	$\gg 10$	>30	10^{11}	-3	Very slight effect
15	>0	$\ll 1$	$<10^{-3}$	10^{12}	6	Negligible effect, states remain filled
16	-2	$\gg 10$	$>10^4$	10^{11}	6	Droop followed by upsweep, detectable
17	-4	$\gg 10$	$>10^5$	10^{11}	6	Droop followed by upsweep, just detectable
18	-6	$\gg 10$	$>10^6$	10^{11}	6	Very slight effect, undetectable
19	-2	$\ll 1$	$<10^{-1}$	10^{11}	6	Small upward displacement, undetectable
20	-4	$\ll 1$	<1	10^{11}	6	Small upward displacement, undetectable
21	-6	$\ll 1$	<1	10^{11}	6	Small upward displacement, undetectable
22	5	$\gg 10$	>10	10^{11}	-2	Droops at end, detectable
23	≤ -4	$\gg 10$	$>10^6$	10^{11}	-2	No effect, states remain essentially empty
24	≤ -4	$\ll 1$	$<10^{-1}$	10^{11}	-2	Slight droop, undetectable
25	≤ -5	$\ll 1$	$<10^{-1}$	10^{11}	-2	No effect, states remain essentially empty

in any way by the sign of charge that the fast states are assumed to have when empty. States at a combination of different energy levels can also be handled by the above technique.

The results listed in Table II apply to n -type Ge where $\Lambda=10^{-1}$, and those in Table III to p -type Ge where $\Lambda=10$. The column entitled "Effect" refers to the effect of the fast states on the photovoltage curve relative to the $N_f=0$ case. The range of χ^2 noted for each case is not critical and can be broadened without affecting the results. For example, in the $T \gg 1$ cases, the lower limit of χ^2 can be decreased an order of magnitude in value. The first conclusion to be drawn from the tables is that the fast states, except in certain cases, have a surprisingly small effect on the photovoltage curves. This indicates that the large-signal photovoltage method is not very well suited for use in studying fast states but, on the other hand, should provide a fairly good indication of surface potential when the fast states are neglected. There is a combination of reasons why the fast states can have a small effect on the photovoltage. Firstly, depending upon ν and Y_0 , the states can remain essentially full or empty. This situation is illustrated by cases 17 and 20 in Table II and cases 1, 23, and 25 in Table III. Secondly, the effect of injection on f in Eqs. (11) and (12) may be such as to compensate for the changes in surface potential occasioned by the injection, so that f remains roughly constant. This is exemplified by cases 1 to 11 in Table II. For any of these reasons the system may move along a nearly horizontal path on the space-charge diagram and the experimenter will be unaware that fast states are present. Because of the exponential or near-exponential relationship between the space charge and the surface potential, the surface potential is relatively unaffected even by fairly large variations in the space charge. In this regard it should be mentioned that the space-charge function for accumulation-layer conditions, with $|Y_0| < 6$ and low-resistivity material, is considerably steeper than that for inversion

layer conditions. This makes the accumulation layer photovoltage even less sensitive to space charge changes than the photovoltage generated under conditions where the surface tends toward an inversion layer. In addition, accumulation layers are less convenient to study because their exploration requires higher carrier injection.

The fast states can have a pronounced effect on the photovoltage when the state level is suitably located and the injection and changing value of Y act on the occupancy factor in the same direction to produce a large combined effect. This situation is exemplified by cases 12 to 16 in Table II and cases 3 to 12 in Table III. However, the altered photovoltage curve may or may not be distinguishable in form from any one of the family of photovoltage curves obtained from a consideration of the space charge alone [Eq. (8)]. In Figs. 9 and 10 are photovoltage curves which illustrate both of these categories. The cases where the curves are clearly distinguishable from the $N=0$ case are shown by the solid curves: the dashed curves illustrate indistinguishable cases. The terms "detectable" and "undetectable" used in Tables II and III refer to the distinguishable and indistinguishable cases, respectively. The allowance for experimental uncertainties is discussed later.

The curves in Figs. 9 and 10 can be qualitatively understood in terms of the limiting forms that the photovoltage curves would take if the fast states were so dense that their effect completely overwhelmed that from the space charge. These limiting forms are obtained from Eqs. (11) and (12) in the same manner that Eq. (8) was derived from the space-charge factor F . Thus, Eq. (11) gives

$$\Delta Y = \ln(1 + \Delta_p), \quad T \gg 1. \quad (13)$$

Equation (12) gives

$$\Delta Y = -\ln(1 + \Lambda^2 \Delta_p), \quad T \ll 1. \quad (14)$$

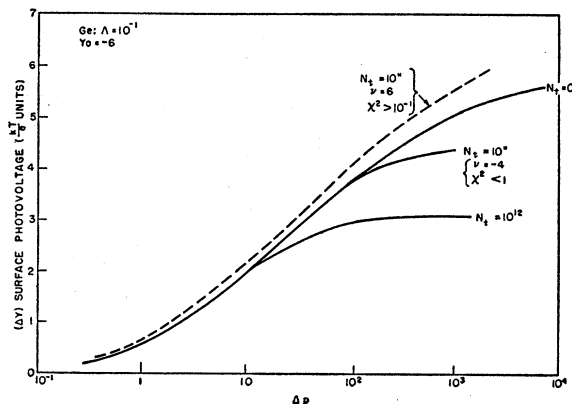


FIG. 9. Effect of fast states on the surface photovoltage. $\Lambda = 10^{-1}$. Solid curves with $N_f \neq 0$ are experimentally distinguishable from the $N_f = 0$ curve, whereas the dashed curve is not.

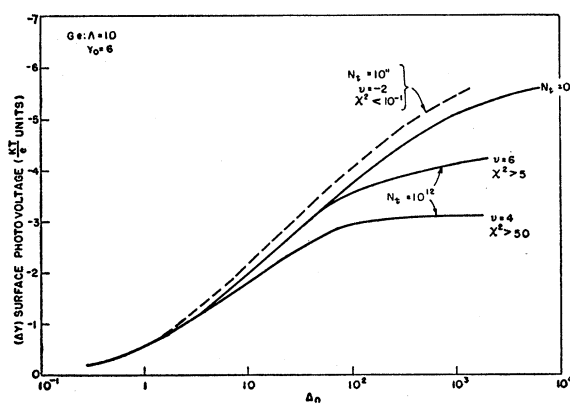


FIG. 10. Effect of fast states on the surface photovoltage. $\Lambda = 10$. Solid curves with $N_f \neq 0$ are experimentally distinguishable from the $N_f = 0$ curve, whereas the dashed curve is not.

These are identical with the limiting forms of Eq. (8), that is, the $|Y_0| = \infty$ curves in Figs. 5, 6, and 7. This explains why the dashed curves in Figs. 9 and 10 lie above the $N_i = 0$ solid curves and have roughly the same shape. The solid curves for $N_i \neq 0$, on the other hand, bend downwards because the fast-state and space-charge photovoltage components oppose each other. Although there are indeed conditions under which the fast states may act to produce photovoltage curves indistinguishable from the family of curves obtained from Eq. (8), consideration of Tables II and III and the preceding argument shows that there is always, at least in principle, a set of surface potential values that will cause the fast-state effect to stand out in a clearly distinguishable manner. This conclusion is less valid for fast states with a continuous distribution of energies. Such states qualitatively affect the photovoltage in the same manner as discrete states, but tend to produce more gradual perturbations of the photovoltage and so would be more difficult to detect.¹⁶ As with the discrete states, the total charge change in the distributed states over the injection cycle would ordinarily have to be at least as large as the space charge itself to produce any significant effect on the photovoltage.

In Figs. 9 and 10 the fast states are seen to have negligible effect on the solid curves at low values of injection. In particular, there is negligible effect at zero injection on the differential photovoltage, that is, on $(dY/d\Delta_p)_{\Delta_n=0}$ and $(dY/d\Delta_n)_{\Delta_n=0}$. This emphasizes the conclusion of Brattain and Garrett who have noted that the differential photovoltage, by itself, can yield little information on fast states because these states merely cause a displacement of the differential photovoltage *versus* Y curve along the Y axis. The expression for the differential photovoltage in the presence of fast states at a discrete energy level can be obtained from Eqs. (5), (6), and either Eq. (11) or (12). When $T \gg 1$, Eq. (11) applies and there obtains

$$\frac{dY}{d\Delta_p} = \frac{\Lambda(e^{Y_0} + e^{-Y_0} - 2) + \Phi}{(\Lambda e^{-Y_0} - \Lambda^{-1}e^{Y_0} + \Lambda^{-1} - \Lambda) + \Phi}. \quad (15)$$

When $T \ll 1$, Eq. (12) applies and there obtains

$$\frac{dY}{d\Delta_p} = \frac{\Lambda(e^{Y_0} + e^{-Y_0} - 2) - \Phi\Lambda^2}{(\Lambda e^{-Y_0} - \Lambda^{-1}e^{Y_0} + \Lambda^{-1} - \Lambda) + \Phi}. \quad (16)$$

The factor Φ , which introduces the effect of the fast states, is defined by

$$\Phi = \frac{2F_0 N_{fs}}{K} [1 + e^{-(Y_0 - \ln \Lambda + \nu)}]^{-2} e^{-(Y_0 - \ln \Lambda + \nu)},$$

¹⁶ Surface nonuniformities, an outstanding uncertainty in this and almost all other surface studies, could introduce similar effects.

where the factor K is 3.5×10^9 for Ge, and 4.0×10^7 for Si. The correct algebraic sign must be used with the factor F_0 as noted in Sec. II. Inspection of Eqs. (15) and (16) will show that their limiting values are consistent with the discussion concerning Eqs. (13) and (14). When $T \gg 1$, the fast states tend to displace the $dY/d\Delta_p$ *versus* Y_0 curves toward positive values of Y_0 ; when $T \ll 1$, the displacement is towards negative values of Y_0 . There is a small effect on the shape of the curves.

The results in Tables II and III might be summarized roughly as follows: with respect to detectability the fast states are ordinarily only detectable when $N_{fs} > 10^{11}$ per cm^2 , $-6 \lesssim \nu \lesssim 6$, and if $Y_0 > 0$ for $T \gg 1$, or if $Y_0 < 0$ for $T \ll 1$. If our attention is confined to surfaces tending toward inversion, since these are more sensitive to fast states in all but intrinsic material and are more convenient to study, we are restricted to detecting states with $\chi^2 \gtrsim 1$ in p -type material, and states with $\chi^2 \lesssim 1$ in n -type material. With respect to producing erroneous conclusions about the surface potential, where this potential is deduced solely on the basis of comparison of the experimental results with the theoretical curves derived from Eq. (8), the states must lie in the range $-6 \lesssim \nu \lesssim 6$ with a density ordinarily exceeding 10^{11} per cm^2 , and must have $Y_0 < 0$ for $T \gg 1$, and $Y_0 > 0$ for $T \ll 1$. Even under very unfavorable conditions the maximum error in potential is only about one kT/e unit. Furthermore, it should always be possible, at least in principle, to find a range of surface potentials that would cause the effect of the fast states to stand out in a distinguishable manner that would serve to caution the observer.

IV. EXPERIMENTAL TECHNIQUE

In these experiments the potential ΔY is picked up by an electrode located close to the surface. This potential is studied as a function of the injection ratio, where the latter is measured from conductance changes in the specimen. The potential ΔY , however, is not the only one that will be detected by the electrode. A Dember potential¹⁷ will be developed in the bulk along the path leading to the reference electrode. This potential is effectively in series with the desired signal of ΔY and arises from the electric field that is set up to equalize the flow rates of holes and electrons diffusing into the bulk from the surface. The value of this potential Y_D can be deduced from the hole and electron flow equations which give, in kT/e units,

$$Y_D = \frac{b-1}{b+1} \ln \left(\frac{R_0}{R} \right). \quad (17)$$

This always appears on the measuring electrode as a positive potential since the Dember, or ambipolar, field always acts to slow down the diffusion of the more mobile carriers (electrons in this case) into the bulk.

¹⁷ W. Van Roosbroeck, Phys. Rev. **101**, 1713 (1956).

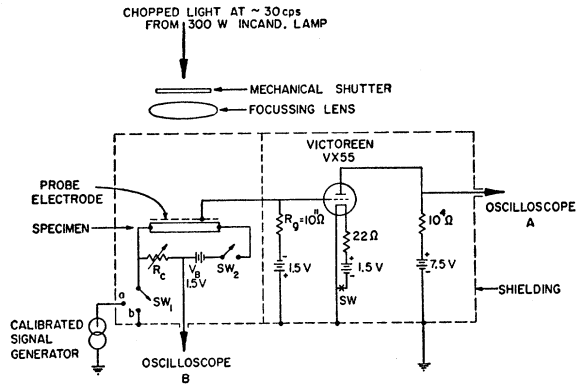


FIG. 11. Experimental arrangement for measurements of surface photovoltage.

The quantity b is the ratio of electron to hole mobility, R_0 is the resistance of a thin specimen in the absence of light, and R is the resistance of the same specimen when illuminated. It will become obvious in the next section that a small error will be introduced into Eq. (17) if the carrier density is not uniform across the specimen. Equation (17) is derived with the assumption, certainly well satisfied in Ge, that there are no appreciable densities of carrier traps in the bulk material.

The potential across the layer wherein the slow and fast states are located could change and contribute to the potential measured by the probe electrode if the charge in this surface region changes or is redistributed. The potential changes that could arise from the charge in the slow states can be ignored because the experiments are going to be carried out so rapidly that this charge cannot change. A rough estimate for the charge in the fast states shows that any potential change from this source should be small except for extreme cases.

The basic experimental arrangement is shown in Fig. 11. Light from a 300-watt incandescent lamp (with built-in reflector), of controlled intensity, is chopped by a disk rotating at a 50-cps rate with a 20% duty cycle. A mechanical shutter allows the light to pass through

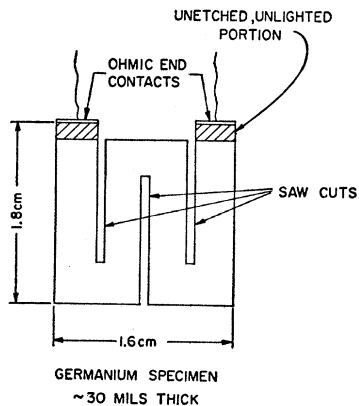


FIG. 12. Specimen geometry.

the lens, a semitransparent electrode, and onto the specimen for periods of time of the order of 0.2 sec (or longer, if desired). This prevents heating of the specimen and reduces the possibility of charge changes in the slow states due to the biasing effect of the light.¹⁸ Measurements showed that the specimen temperature rise during a reading was never greater than 0.2°C. The probe electrode is a thin perforated piece of nickel with an optical transparency of approximately 50%. The electrode can be separated from the specimen by air or by some well-behaved dielectric like mica. Systematic comparison of both air and mica dielectrics showed no significant difference between the two. The spacing was a few mils.

With switch SW_1 on position b and switch SW_2 open, the surface photovoltage ΔY is passed through the electrometer tube preamplifier to oscilloscope A . The surface photovoltage signals observed in these experiments ranged up to a few hundred millivolts. After the amplitude of the surface signal is noted on the oscilloscope, the light is removed and a calibrating signal is fed in from the calibrated signal generator which operates at the light chopping frequency. This gives an absolute calibration of the surface signal. This, after correction for the Demer potential obtained from Eq. (17), is equal to the surface photovoltage ΔY . The wave shape of the surface signal is closely approximated by feeding the sinusoidal wave from a standard audio signal generator through a semiconductor diode used as half-wave rectifier. This refinement, however, is hardly necessary. The back contacts on the specimen should be made as ohmic as possible and should be shielded from light to eliminate photovoltaic effects.

In determining the injection factor Δ_n or Δ_p from specimen resistance changes, there are two corrections to be made. First of all, there is the end resistance of the specimen, i.e., the portion of the total specimen resistance that is not involved in the light-induced resistance change. This is always present when the end contacts are shaded from the light. This resistance, amounting to roughly 5 or 10% of the total specimen resistance in these experiments, can be estimated from geometrical considerations or from probe measurements carried out on the unlighted specimen. This correction is of importance only at high injection levels when the total specimen resistance becomes small. Secondly, when the specimen is not thin compared to a bulk diffusion length a correction has to be made for the fact that the excess carrier density near the surface is larger than the average density, necessarily measured from the resistivity change. For these experiments this correction factor was roughly 1.5. The battery potential V_B , noted in Fig. 9, is well below the value that would introduce error from carrier sweep-out effects at the end contacts. The assumption that the carrier mobilities remain constant during heavy injection will introduce

¹⁸ S. R. Morrison, Phys. Rev. **102**, 1297 (1956).

negligible error under the conditions of these experiments.¹⁹

The Ge specimens were cut from 30-mil thick rectangular blanks in the configuration shown in Fig. 12. The saw cuts transformed the rectangular specimen into one with a long current path leaving, at the same time, a specimen surface area of convenient shape and size. All etching and exposure to light was limited to the surfaces below the cross-hatched ones. This prevents possible trouble from end contact material dissolving in the etch and, also, helps insure freedom from photovoltaic effects at the contacts. The specimens were treated by the usual CP4 etch, washed in triple distilled water, and then dried with hot air.

V. EXPERIMENTAL RESULTS AND COMPARISON WITH THEORY

Figure 13 shows data taken with a *p*-type Ge specimen (No. 2) whose resistivity (12 ohm-cm) corre-

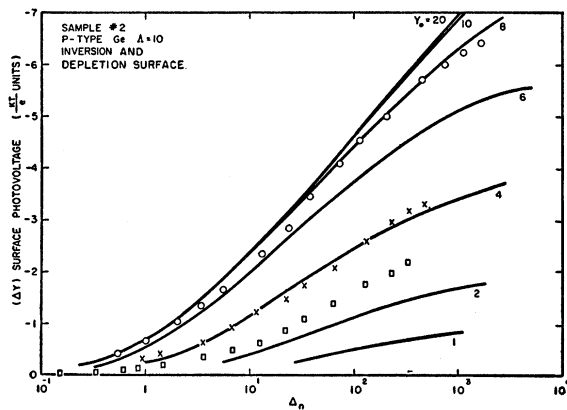


FIG. 13. Experiment and theory for *p*-type Ge with $\Lambda = 10$. Inversion layer tendency.

sponded to $\Lambda = 10$. The solid curves, corresponding to surfaces tending toward inversion, are computed from Eq. (8). The three runs of experimental data, denoted by the circles, crosses, and squares, were typical of many runs made on sample No. 2. The circles correspond to the case where the specimen was etched, washed, dried, and then exposed to room air (~65% RH).²⁰ The crosses and squares refer to the cases where the specimen was subjected to varying flows of dry O₂. The close similarity of form between the experimental data and the theoretical curves based on the space charge suggests that both are in accord. This implies, for the case marked by the circles, that $Y_0 \approx 8$; for the crosses, $Y_0 \approx 4$; and, for the squares, $Y_0 \approx 3$.

¹⁹ This can be deduced from the paper of M. B. Prince, Phys. Rev. 92, 681 (1953).

²⁰ As in the many other case observed, a Ge surface almost always tends toward *n*-type after etching and the subsequent washing and drying operations. With reference to the known results of the wet-dry O₂ cycle, this implies that some water remains on the surface even after a vigorous drying operation.

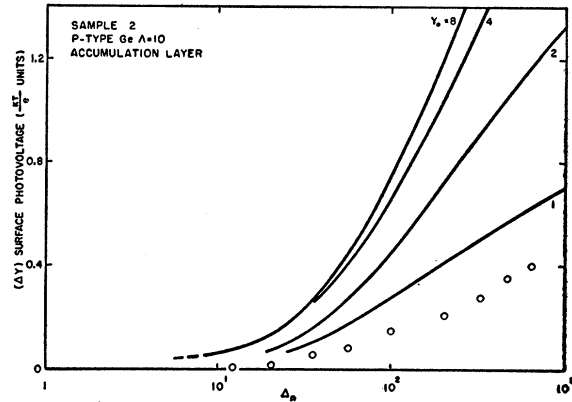


FIG. 14. Experiment and theory for *p*-type Ge with $\Lambda = 10$. Accumulation layer.

When dry O₂ and ozone were applied to the specimen, accumulation-layer conditions developed on the surface giving the typical data shown in Fig. 14: note the change in vertical scale. The solid curves are the theoretical ones corresponding to accumulation-layer conditions and were taken from Fig. 5.

These experiments are sometimes difficult to perform because each experimental run must be completed before the labile equilibrium between the surface and the surrounding ambient atmosphere causes a significant drift in the surface potential. The experiments could have been facilitated by using (1) a light source modulated over the appropriate intensity range at a 60-cps rate, and (2) a camera to record the traces on oscilloscopes A and B (Fig. 11).

The theoretical curves and the data shown in Fig. 15 apply to surfaces tending toward inversion on an *n*-type specimen (No. 3) whose resistivity of 7 ohm-cm corresponds to $\Lambda = 10^{-1}$. The different runs correspond to different points of the ambient cycle. The bottom two runs were made in the presence of fairly wet air. Again it is seen, with the exception of the bottom run, that there is conformity between theory and experi-

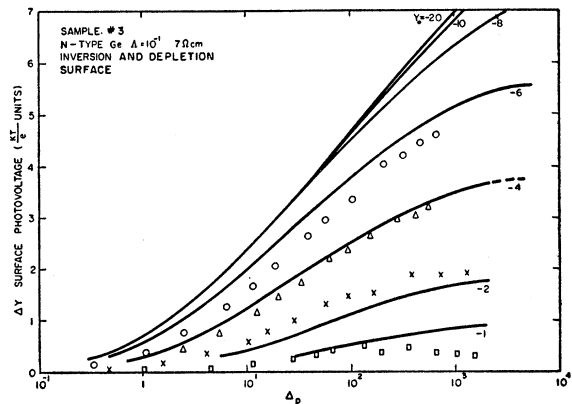


FIG. 15. Experiment and theory for *n*-type Ge with $\Lambda = 10^{-1}$. Inversion layer tendency.

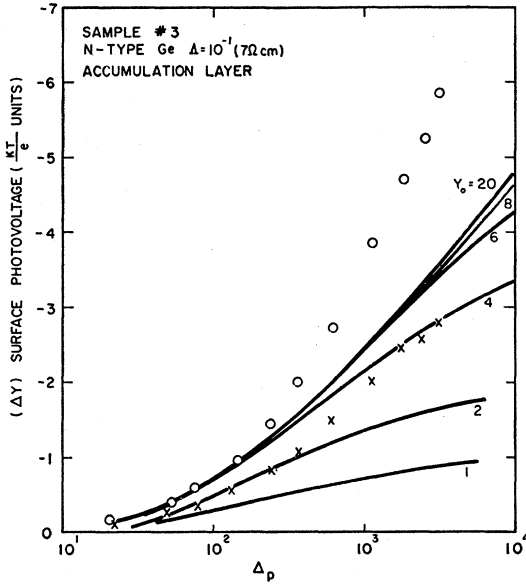


FIG. 16. Experiment and theory for *n*-type Ge with $\Lambda=10^{-1}$. Accumulation layer.

ment. Even the bottom run behaves properly at values of Δ_p less than 10^2 . The deviation at higher values of Δ_p is real and stems, it is believed, from changes in the charge of the slow states. This belief is based on the fact that there is a greatly enhanced tendency for light-injected carriers to bias the surface potential when the surface is exposed to moisture. This biasing action showed up, in the case in question, as a tendency for the surface photovoltage to drift to lower magnitudes, particularly at higher carrier injection levels. It also shows up as an overshoot in the oscilloscope signal. These observations are consistent with the wet ambient-induced reductions in the slow-state time constant that have been observed elsewhere.^{21,22}

It is easily deduced from curves of the sort shown in Fig. 8 that the sagging characteristic of the bottom run corresponds to an increase in the negative charge in the slow states. This conclusion is further emphasized by the behavior of the data in Fig. 16, which applies to the same sample under accumulation-layer conditions where the surface was subjected to an extreme point on the wet part of the ambient cycle. Here the marked departure of the data from the theoretical curves, where $\Delta_p > 2 \times 10^2$, can also be interpreted as an addition of negative charge to the slow states.

The data in Fig. 17 which apply to a surface tending toward inversion on an *n*-type Ge sample (No. 1), where the 1.1 ohm-cm resistivity corresponded to $\Lambda=1.7 \times 10^{-2}$, show conformity between theory and experiment. There is, again, a noticeable sagging effect on the run, marked by the crosses, which corresponded

²¹ R. H. Kingston and A. L. McWhorter, Phys. Rev. **103**, 534 (1956).

²² G. C. Dousmanis, private communication (to be published).

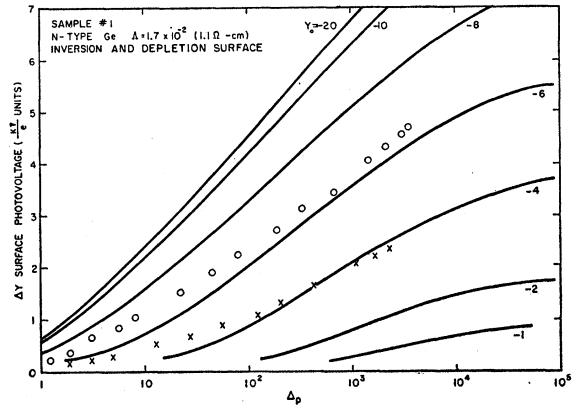


FIG. 17. Experiment and theory for *n*-type Ge with $\Lambda=1.7 \times 10^{-2}$. Inversion layer.

to conditions where there was an increase in the humidity.

The different samples tested often varied widely in their sensitivity to ambient changes. As a rule, however, high-resistivity samples tended to give wider variations in surface potential for given ambient changes than the low-resistivity ones.²³

Rapid, approximate, determinations of the surface potential can be carried out once a rough calibration of the minority carrier injection factor is obtained. It is obvious from the photovoltage curves that the minority carrier injection factor, at large values, can vary over wide limits without affecting the value of Y_0 that would be deduced from a single point measurement.

It is to be emphasized that there are no adjustable parameters of any kind in the experimental data. The end-resistance corrections for the carrier injection factor in Fig. 13 are negligible below $\Delta_n=50$ and increase to about 50% at the maximum value of Δ_n . Roughly the same values hold for Fig. 15. The maximum end-resistance correction for the data in Fig. 17 is about 15%. The Dember correction is of opposite sign in Figs. 13 and 15 and amounts to about $0.8kT/e$ unit at the maximum values of the surface potentials. This correction, however, is negligible for the data in Fig. 17. It can thus be seen that the data were collected over a fair range of the various correction factors.

An incidental observation was that the surface recombination velocity s in samples Nos. 2 and 3 was essentially constant over the range $|\Phi_s| \leq 4$. This was deduced from the behavior of the excess carrier density under constant light level conditions. In sample No. 1, however, s rose rather rapidly as Φ_s varied from -3 to 0 , the range covered by the data on this particular sample.

VI. DISCUSSION

Except for the cases where there is good reason to suspect a change in the slow-state charge, the observed

²³ Similar observations have been made by F. Rudo and J. Hammes of the RCA Semiconductor Division.

surface photovoltage seems to be in good accord with the behavior predicted from a consideration of the charge redistribution in the surface-charge region. The excursions of the surface potential over the ambient cycle seem to be at least as large as those previously reported⁷: *p*-type Ge, $Y_0 = -2$ to $+8$; *n*-type Ge, $Y_0 = -6$ to $+4$. The bunching together of the photovoltage curves at higher values of Y_0 makes estimates of the extreme values of Y_0 uncertain. Thus, there is not necessarily any conflict with the relatively large swings of surface potential that are indicated in these laboratories with the back-diode method.²²

In none of the measurements, at least within what is believed to be the probable accuracy, was there any evidence for charge change in the fast states. This fact will be used below to derive conclusions about the possible energy levels and density of these states.

The error in the carrier injection factor could be, perhaps, as high as 50% at high levels because of the uncertainty in the correction for the specimen and resistance. At low and intermediate injection levels this correction is unimportant so that the error is much smaller. The value of Δy might be in error by as much as 10%. These fairly conservative estimates of possible error make the surface potential Y_0 uncertain by roughly one-half to one kT/e unit. This is about the same error that could stem from fast states, whose effect is to displace the photovoltage curve without producing enough change in its shape to make it clearly distinguishable from the family of curves computed from Eq. (8).

First of all, the results of this study lead to the conclusion that, unless the measurements cover a large range of Y_0 (both accumulation and inversion layers), the large-signal technique is not a good general method for studying fast surface states. Only states with a certain combination of parameters can be detected.

On the other hand, the relative insensitivity of the photovoltage to fast states indicates that the method should be fairly reliable for determining the surface potential to within about one kT/e unit when the fast states are completely neglected. The experimental technique for determining surface potential is simple, straightforward, and completely independent of uncertainties in the carrier mobility near the surface. Unfortunately the method loses accuracy for surface potentials (Y_0) in excess of about $8kT/e$ units for surfaces tending toward inversion and about $4kT/e$ units for accumulation surfaces. The method has the further disadvantage of being adversely affected by the slow-state charge changes that occur with wet ambients.

The good conformity between the experimental photovoltage curves, observed over a fair range of experimental conditions, and those derived from the space-charge relation, leads to the following rough conclusions about fast states: In the *n*-type Ge there could not have been any states of a density greater than a few times 10^{11} within $6kT/e$ units from gap center, if these states had a small value of χ^2 . The condition that χ^2 not be unreasonably small ($\lesssim 10^{-3}$) restricts the statement to states above the gap center. Slow-state charge changes introduced by water vapor make it difficult to draw any conclusions from runs with accumulation layers. This rules out the possibility (see Table II, case 21) of detecting states below midgap with $\chi^2 \gtrsim 10^2$. In the *p*-type Ge there could not have been any fast states, with $\chi^2 \gtrsim 1$ and a density greater than about 10^{11} , located in the energy range from gap center to about $6kT$ below gap center. The maximum error in surface potential caused by possible undetected fast states very likely lies within the probable experimental uncertainty of one-half to one kT energy unit.

In Table IV is compiled the detectability of previ-

TABLE IV. Previously reported discrete fast states (germanium).

Case	Reference	Sample type	resist. (ohm-cm)	ν (kT/e units)	State N_t (No./cm ²)	χ^2	Remarks
1	4	<i>N</i>	1	5.5	1.4×10^{11}		Undetectable if $\chi^2 \gtrsim 1$
2	5	<i>P</i>	1	-5.2	$10^{10} - 10^{11}$	≥ 10	Undetectable
3	5	<i>P</i>	1	-7.2	$10^{11} - 10^{12}$	≥ 10	Undetectable
4	3	<i>N</i>	35	-3.9	4×10^{10}	10	Undetectable
5	3	<i>N</i>	35	1.65	4×10^{10}	10	Undetectable
6	3	<i>N</i>	35	< -6	$> 8.8 \times 10^{10}$		Detectable if $\chi^2 \approx 1$ and $N_t \approx 10^{12}$
7	3	<i>N</i>	35	> 5	$> 1.1 \times 10^{11}$		Undetectable if $\chi^2 > 1$ and $N_t \approx 10^{12}$
8		<i>N</i>	35	-3.9, or 1.65	10 ¹¹	10)	Aggregate not detectable unless $N_t \approx 10^{12}$
					5		
					10 ¹¹		
9	24	<i>N</i>	17	5 to 6	1.3×10^{11}		Undetectable if $\chi^2 \gtrsim 10^{-1}$
10	24	<i>N</i>	17	< -5			Detectable if $\chi^2 \lesssim 10$, $N_t = 10^{12}$, otherwise undetectable
11	25	<i>N</i>	20	-4.8	($\sim 10^{11}$) ^a	30	Undetectable at $N_t = 10^{12}$
12	25	<i>P</i>	19.5	-4.8	($\sim 10^{11}$) ^a	30	Undetectable at $N_t = 10^{12}$
13	25	<i>N</i>	25	-6	($\sim 10^{11}$) ^a	150	Undetectable at $N_t = 10^{12}$
14	25	<i>N</i>	25	9	($\sim 10^{11}$) ^a	4.5×10^{-5}	Detectable at $N_t = 10^{12}$
15	22	<i>N</i>	0.3-3.0	± 8		~ 1	Undetectable, unless $\nu = -8$ and $N_t \approx 10^{12}$

^a A. Many, private communication (to be published).

ously reported^{3-5,22,24,25} fast states. In some cases the detectability could be inferred from the results in Tables II or III, and in other cases additional calculations were necessary. The criterion for detectability is the same as that discussed in Sec. III; the allowance for experimental uncertainties is established earlier in the present section. Some liberties are taken with the fact that some of the resistivities noted in Table IV are outside the range of those used in the present study. These differences should not affect any of the conclusions. It has to be assumed, of course, that the surfaces were all comparable to those present on the samples used in the present study.

It is seen that the results of the present study, with only minor qualifications, are at least consistent with those extant in the literature. In cases 6, 9, and 13, certain limits are placed on the state densities and capture cross-section ratios. Case 8, which refers to the aggregate of states listed under reference 3 in the table, was included because these states, taken together, provide a good approximation³ to the fast-state charge curves^{2,15} from which continuous energy distributions have been inferred. In the absence of more complete information, the values noted in the table for N_t and χ^2 were used. The computed effect of this aggregate of states both on the large signal photovoltage and on the

differential photovoltage, as described by Eqs. (15) and (16), was found to be negligibly small unless the state densities in this case were increased to about $10^{12}/\text{cm}^2$.

VII. CONCLUSIONS

The large-signal surface photovoltage is insensitive to fast states over a considerable range of state parameter values. Hence the technique described in this paper is not a good one to use in general studies of these states. However, on the other hand, the insensitivity to fast states seems to make the technique a fairly reliable tool for determining surface potential, at least in Ge. It is convenient to use and is not affected by uncertainties in carrier mobilities along the surface. The range of insensitivity to fast states includes the state parameter values listed in the literature; the range of sensitivity includes parameter values which are not listed in the literature. Since no evidence for fast states was observed in the present study, it is concluded that the results of this study are at least consistent with previously reported fast-state parameters.

ACKNOWLEDGMENTS

The author is indebted to G. C. Dousmanis who made many helpful suggestions, and to S. Skillman who carried out machine evaluations of the surface space-charge relations. It is a pleasure to acknowledge the many valuable comments of C. G. B. Garrett of the Bell Telephone Laboratories.

²⁴ Bardeen, Covert, Morrison, Schrieffer, and Sun, *Phys. Rev.* **104**, 47 (1956).

²⁵ Many, Harnik, and Margoninski, in *Semiconductor Surface Physics* (University of Pennsylvania Press, Philadelphia, 1957), pp. 85-107.